JOURNAL OF AIRCRAFT
Vol. 39, No. 1, January–February 2002

# Wind-Tunnel Testing of the Wright Brothers' Model B Airfoil

Drew Landman,* Julian Alvarez,† Robert Ash,‡ and Spiros Blackburn†
*Old Dominion University, Norfolk, Virginia 23505*
and
Ken Hyde§
*The Wright Experience, Warrenton, Virginia 20187*

**Wind-tunnel tests of a Wright Model B airfoil have been conducted using two-dimensional models in full- and third-scale at flight Reynolds numbers. In an effort to ascertain the effect of rib and covering construction on airfoil aerodynamics, the full-scale model was fabric covered and maintained the original dimensions of the Wright Model B Flyer wing. Because the full-scale model could only be tested over a small angle-of-attack range, a solid surface, third-scale pressure model was constructed. Lift and pitching moment polars from the tests are presented over a range of angles of attack spanning zero lift to poststall. A drag polar is presented for an angle-of-attack range from −4 to 6 deg. Surface static pressure distributions are presented from the third-scale model. Flow visualization study results show separation on the bottom surface for angles of attack below 0 deg and on the top surface for angles of attack above 6.5 degrees. The Wright wind-tunnel tests of 1901 are shown to have given excellent correlation for lift values when compared to the present test.**

## Nomenclature

| | | |
|---|---|---|
| AR | = | aspect ratio of rectangular wing (span/chord) |
| $C_L$ | = | lift coefficient (AR finite), $L/qS$ |
| $C_l$ | = | lift coefficient (AR infinite), $L/qc$ |
| $C_{m1/4}$ | = | pitching moment coefficient (AR infinite), $M/qc^2$ |
| $C_p$ | = | pressure coefficient, $(P - P_\infty)/q_\infty$ |
| $c$ | = | airfoil cord length |
| $L$ | = | lift |
| $P$ | = | local static pressure |
| $P_\infty$ | = | freestream static pressure |
| $q_t$ | = | wind-tunnel freestream dynamic pressure |
| $q_w$ | = | dynamic pressure in airfoil wake |
| $q_\infty$ | = | freestream dynamic pressure |
| $Re_c$ | = | chord Reynolds number, $\rho V c/\mu$ |
| $V$ | = | velocity |
| $x$ | = | chordal spatial coordinate |
| $x_{cp}$ | = | center of pressure, $\frac{1}{4} - C_{m1/4}/C_l$ |
| $y$ | = | vertical spatial coordinate of wake survey |
| $\alpha$ | = | angle of attack |
| $\mu$ | = | viscosity |
| $\rho$ | = | density |

## Introduction

THE Wright Experience, Old Dominion University, Wichita State University, and NASA Langley Research Center (LaRC) sponsored two wind-tunnel tests on a Wright Model B airfoil geometry. The Model B, the first production Wright aircraft, has the most complete engineering specifications and documentation available and was chosen as the first test article in a planned series of tests to evaluate the performance of early Wright aircraft. The Model B reproduction is to be airworthy, and after wind tunnel evaluation of the full-size aircraft, flight-simulator and flight-test evaluations are planned to fully document the Model B's handling qualities including use of the unique flight controls. The overall test program, aimed at eventually flying a true 1903 reproduction, will proceed by moving back in time from the 1910 Model B. The Wright Experience has been chosen by the Experimental Aircraft Association to build the National Park Service's 1903 flightworthy, exact reproduction for the centennial celebration of the Wright's first flight at Kitty Hawk, North Carolina.

This paper presents wind-tunnel test results from full-scale and third-scale two-dimensional airfoil tests conducted at the National Institute for Aviation Research (NIAR) and LaRC, respectively. It is hoped that the data from this test will benefit not only the current program but also provide a historically significant database for Wright airfoils.

## Historical Background

After Wilbur Wright's invention and subsequent demonstration of wing-warping roll control, in the summer of 1899, he and his brother Orville decided they would attempt to build a manned glider. The Wright brothers planned to exploit the existing airfoil literature of that time,[1,2] and by the early fall of 1900, they had built and flown their first piloted glider. With the use of airfoil data of Lilienthal[3] as their primary basis for design, they used flight-test results from their glider flights at Kitty Hawk, North Carolina, to design a larger improved glider for their 1901 test campaign. In addition to identifying serious lateral control issues, the 1901 glider flight tests included lift measurements, where it was found that they had underpredicted lift by at least 20%. Wilbur and Orville became convinced that there was something wrong with the published literature. After returning to Dayton, Ohio, in the fall of 1901, the Wright brothers embarked on an ambitious wind-tunnel-based testing program that enabled them ultimately to explain most of the inconsistencies between their measured glider performance and their predictions utilizing published literature. Their experimental investigations in late 1901 and early 1902 enabled them to develop an aircraft design approach[2] that led to their successful powered flights in December of 1903 and gave them a technological advantage over their competition.

Anderson[4] has discussed how the Wright brothers untangled their technical difficulties relating to predicting performance, ranging from estimating dynamic pressure (using Smeaton's constant) to their utilization of Lilienthal's[3] tabulated airfoil data. Their

Received 13 April 2001; revision received 28 August 2001; accepted for publication 15 September 2001. 

*Assistant Professor, Department of Aerospace Engineering. Senior Member AIAA.
†Graduate Research Assistant, Department of Aerospace Engineering. Student Member AIAA.
‡Eminent Scholar, Department of Aerospace Engineering. Member AIAA.
§Owner, Director.

wind-tunnel tests enabled them to estimate their airfoil performance with sufficient accuracy to design and build a powered flying machine in 1903. Anderson[4] contends that there were three sources of error or misunderstanding that contributed to the Wright's early design difficulties: 1) They overestimated the dynamic pressure by 40%. 2) They did not understand the influence of aspect ratio and camber on aerodynamic coefficients. 3) They did not understand how the location of airfoil center of pressure could be controlled. Anderson noted also that the Wright brothers, like their contemporaries, did not understand the influence of Reynolds number on airfoil model-test scale up. There can be little disagreement with Anderson; however, note that the Wright brothers adopted circular arc and parabolic contours for their flying machine airfoils, of the type tested and reported by Lilienthal,[3] rather than the unusual airfoil cross sections sketched in some of their early correspondence.

Historians have speculated that the Wright brothers based many of their aerodynamic designs on one of their wind-tunnel airfoils, designated as *number 12*, when tested in December of 1901. That airfoil was a parabolic section with a camber of $\frac{1}{20}$, and it had a maximum camber location that was forward of the chord midsection. The machine digitized representation of the ribs used in the Model B, on display at the Franklin Institute in Philadelphia, coincide with their airfoil model *number 12*. The measured maximum camber occurs at approximately 41% of the chord. A preliminary examination of the 1903 Flyer ribs (before a digitized comparison) indicates that the rib contours are similar to the Model B ribs, except that the Model B ribs were of constant depth (4,445 cm) over the first two-thirds chord, behind the forward spar. The remaining one-third chord of the Model B ribs were tapered to the trailing edge, whereas the 1903 ribs were tapered continuously from the forward spar to the trailing edge. The *number 12* airfoil test of 1901 used a wing of chord length 2.54 cm and an aspect ratio of 6 (Ref. 1). Note that Wright brothers' wind-tunnel airfoil models, were made from a single surface of 20-gauge steel sheet (constant thickness); therefore, their decision to vary the rib thickness was not based on their model tests. This does add some ambiguity in comparing data to the Wright's airfoil tests.

## Model B

The Model B flyer, first produced in 1910, is shown in Fig. 1. This biplane had an overall length of 8.53 m and a gross weight of 567 kg. The wing spanned 11.89 m with a chord of 1.88 m and area of 46.5 $m^2$ (Ref. 1). Propulsion was provided by a single 29.1 kw engine that drove two counter-rotating pusher propellers through a chain drive. Control was through dual levers that moved fore and aft. One lever provided pitch control through a full flying stabilizer and the other coupled roll and yaw control through wing warping and a full flying rudder.[5] In addition, a small secondary handle on the lateral control stick allowed trimming the rudder in turns.

Although the airfoil geometry looks similar to the 1903 Wright Flyer, they are quite different. The leading edge radii are identical, but the 1903 airfoil thickness tapers continuously along the chord line where the Model B is constant thickness, until the trailing spar, where it then tapers to the trailing edge. The Model B wing design is consistent with the 1903 design in that the load is carried by the leading-edge spar and a trailing spar. The covering on the Model B is

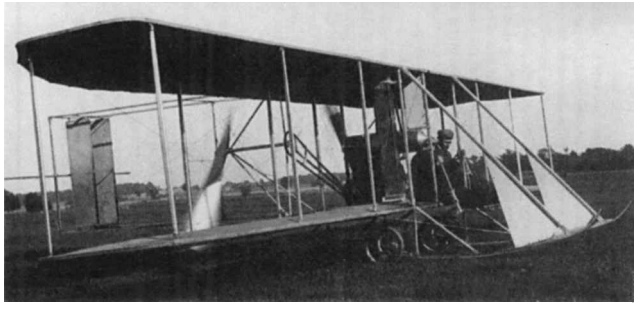

**Fig. 1 Wright Model B Flyer (1910).**

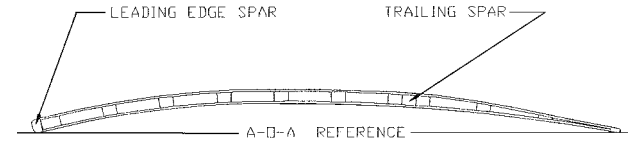


**Fig. 2 Model B airfoil showing spar locations and angle-of-attack reference line.**

attached to the bottom surface of the ribs via a pocket sewn into the fabric; the top surface fabric was not attached to the ribs, but only to the leading-edge spar and to a trailing-edge wire. The hardened steel wire was encased in a pocket sewn into the trailing edge of the fabric covering, which was pulled tight to give the scalloped appearance in the wing plan view. The rib design consists of two cap strips and various spacing blocks as shown in the end view of Fig. 2. The camber is $\frac{1}{20}$, and the camber line follows an approximate circular arc.

## Test Philosophy

The unique wing covering arrangement suggested a need for full-scale modeling of the airfoil to capture the aerodynamic effects of the suspected top surface fabric deformation. In particular, the fabric effect on minimum drag and cruise lift coefficient were of great interest to planned aircraft performance simulations. Unfortunately, the size of the chord prohibited full-scale testing of the airfoil in traditional two-dimensional airfoil testing facilities. A search for available facilities with adequate two-dimensional test section areas to allow a full angle-of-attack sweep without excess blockage proved unsuccessful. Because the project budget fell short of constructing a two-dimensional insert for existing large-scale facilities, it was decided to proceed with this test in two phases. A full-scale model was constructed for use in a $2.13 \times 3.05$ m test section restricted to a limited angle-of-attack sweep. A second model was constructed at one-third scale for use in a traditional two-dimensional airfoil test facility. In this manner, the effects of the fabric could be ascertained for the typical operating range of the aircraft and compared to the complete polar of the third-scale model.

The Walter H. Beech Memorial $7 \times 10$ Foot Low Speed Wind Tunnel at Wichita State University (WSU $7 \times 10$) was used for full-scale testing. A floor to ceiling model was constructed to span the 2.13 m height of this $2.13 \times 3.05$ m test section. Lift data were obtained with the floor to ceiling force balance and drag data using a wake rake. The LaRC Low Turbulence Pressure Tunnel (LTPT) was chosen for the excellent flow quality and ability to pressurize the test section to achieve flight Reynolds numbers with a relatively inexpensive model structural requirement. Lift and pitching moment data were obtained using surface pressures and drag data with a wake rake. Surface flow visualization was conducted using wool or thread tufts in both facilities. Both airfoil models were designed to be tested at the cruise flight Reynolds number of $2.6 \times 10^6$.

## Airfoil Models

### Load Prediction

A literature search for existing data on any Wright airfoil was conducted with controversial results because the references did not clearly identify which Wright airfoil geometry was tested. Uncertainties associated with load prediction, and a lack of published pressure distribution data (to place model pressure orifices better), necessitated computational analysis using smoothed, measured coordinates from a reproduction rib with Airfoil II™.[6] The computational Model B geometry had to be modified for code convergence due to the unusually blunt leading edge and thick trailing edge. The original and modified geometry used with a successful Airfoil II run are shown in Fig. 3. The lift polar from the Airfoil II model using the flight Reynolds number of $2.6 \times 10^6$ is included with the available reference data in Fig. 4. The poststall portion of the curve is an artifact of this coupled boundary-layer–inviscid flow method, which was never intended to model the large-scale separation that occurs on the Wright airfoils. The curves labeled Wright 12 and 18 are taken from the Wright brother's original notes published in Ref. 1. The data comes from the Wright's 1901 wind-tunnel tests on small

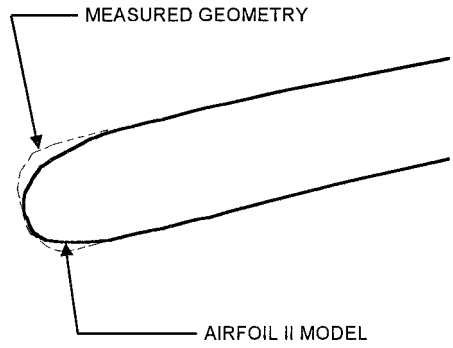


**Fig. 3 Comparison of measured rib geometry to Airfoil II model at the airfoil leading edge.**

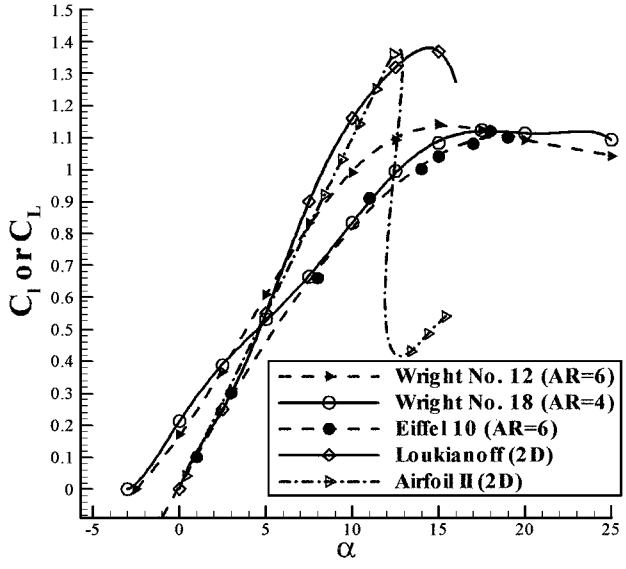


**Fig. 4 Reference lift data.**

wings at a fixed Reynolds's number of $5.8 \times 10^4$. The data noted as Eiffel 10 in Fig. 4 were taken at the Eiffel Laboratory from a wing model of aspect ratio 6 at a Reynolds number of $1.03 \times 10^5$ in 1913 and published by NACA in 1921, labeled as a Wright profile.[7,8] The curve labeled Loukianoff is data originally published in 1912 for a model of 0.5-m chord with an aspect ratio of approximately 0.6, tested at a Reynolds number of approximately $6 \times 10^5$ (Ref. 9). From the reference data, a lift coefficient of approximately 1.4 was chosen as a safe maximum to use for model structural design considerations. A sample pressure distribution from the computational model is shown in Fig. 5 and reveals characteristic leading-edge peaks on the top and bottom surface and the relatively constant pressure regions from $x/c = 0.20$ to the trailing edge. These pressure distributions suggested the possibility of a laminar leading-edge separation bubble.[10]

### Full Scale

The balance system of the NIAR 7 × 10 relies on a rigid-model design to ensure accurate in situ calibration. To this end, a steel spar structure with aluminum ribs was designed for minimum model deflection. Model B rib reproduction tooling was created by The Wright Experience to manufacture the wing. Coordinates for the rib jigs were obtained by measuring ribs from a surviving Wright Model B wing panel and an isolated rib from a second source. A newly manufactured reproduction rib was then measured using a coordinate measuring machine and the data set used to produce tool paths for computer numerical controlled milling of the ribs. The reinforced design maintained the geometry of the original covered wing, with the exception of rib spacing at the ends. The covering material was identical with the material used on the 1910 aircraft, a rubberized cotton, and it was attached to the ribs in the same

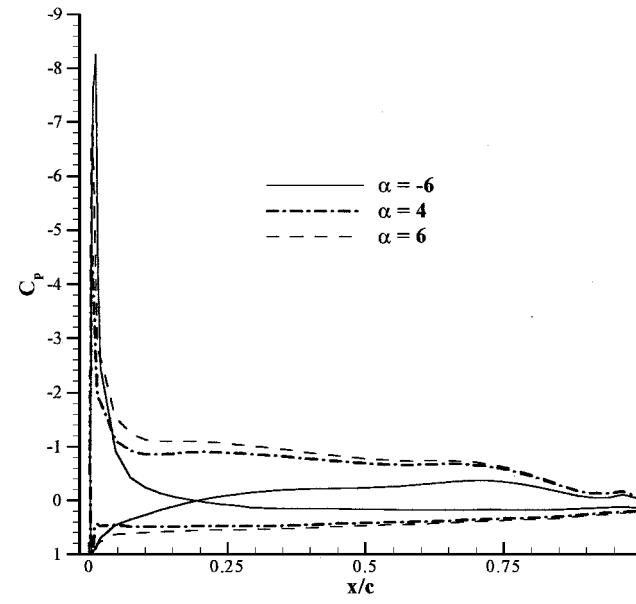


**Fig. 5 Sample of Airfoil II predicted pressure distributions.**

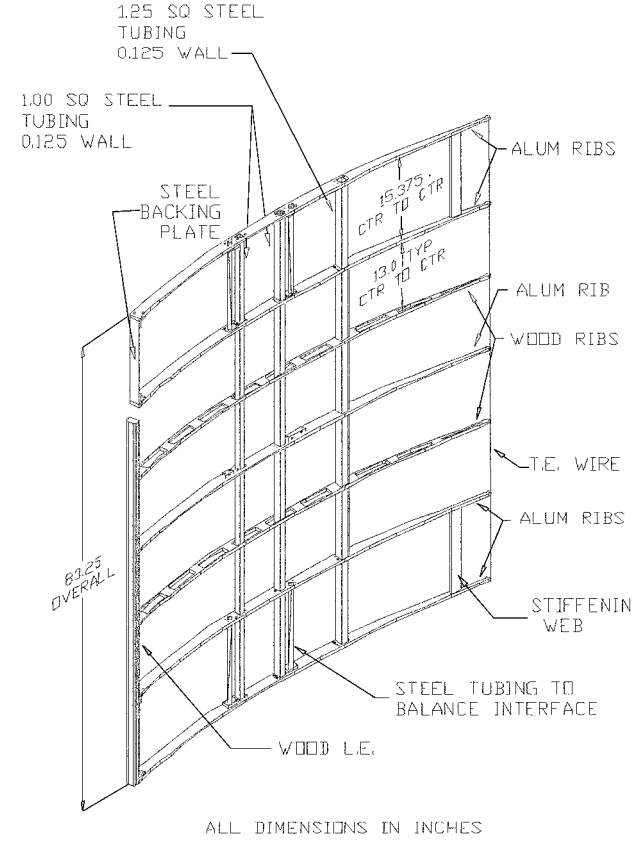


**Fig. 6 Full-scale Model B airfoil model design.**

manner as the original.[11] The wooden leading edge was reproduced to allow nailing of the top surface covering material. Fabric rib pockets were used on the lower surface, and a trailing-edge wire secured the trailing-edge fabric as in the original. The model is shown in Fig. 6.

### Third Scale

The third-scale model was of composite design utilizing a steel main and auxiliary spar system, aluminum end ribs, a structural foam core, and a fiberglass and epoxy resin covering. Mounting tangs were attached to the end ribs for use in the LTPT. The aluminum ribs were computer numerical machined using the scaled

geometry from the full-scale model. The foam was rough cut and glued to the rib assembly using a mix of epoxy and fairing filler, which was then carefully shaped to profile using a large sanding bar with the end ribs as guides. Pressure tubing channels for 31 surface orifices were routed into the foam core, glued, and filled, before the fiberglass skin was applied with a vacuum bagging technique. Pressure orifices were then drilled into the surface of the model, through to the underlying tubing.

## Experimental Details

Angle of attack is referenced to a line of tangency on the airfoil bottom surface, found by positioning the model on a flat surface as shown in Fig. 2.

### Full Scale

The WSU 7 × 10 is a closed return, atmospheric pressure, closed throat, 2.13 × 3.05 m rectangular test section low-speed wind tunnel. The large-scale two-dimensional airfoil balance system relies on strain gauge load cell force measurements in both the floor and ceiling, spanning the 7-ft height. This system is capable of measuring lift, drag, and pitching moment. Test section calibrations for the dynamic pressure show a turbulence factor of approximately 1.4, buoyancy of $-0.0180\,C_p$/m, and flow angularity of less than 0.1 deg over the entire test section area.[12] In this experiment, the dynamic pressure was chosen based on the full-scale Reynolds number of $2.6 \times 10^6$ and averaged approximately 316 Pa. The relatively low forces at these conditions required the measurement of drag by wake survey, accomplished using a fixed rake of total pressure probes with tube spacing of 318 cm. The rake was constrained to operate at a distance of 44.5 in. downstream of the trailing edge. Pressures were measured using a PSI 8400 electronic pressure scanner with a range of 17.2 kPa differential (psid) calibrated using a 6.89 kPa range precision unit. Lift forces were sampled from the load cells using a Hewlett–Packard Company 3852 data acquisition system. Tufts on both surfaces were filmed during the test with video recorders for posttest analysis. A pretest evaluation of the boundary corrections incurred over an angle-of-attack sweep from −4 to 4 deg, using the predicted forces and the method of Ref. 13, showed that it was possible to measure the lift and drag coefficients with less than a 15% correction at the limits.

### Third Scale

The LTPT is a pressurized, closed throat, 9144 × 2.286 m rectangular test section wind tunnel purposely designed for two-dimensional airfoil testing. A test section pressure of 4 atm was selected to achieve a Reynolds number of $2.6 \times 10^6$ while maintaining relatively small loads on the model. At this operating pressure, the approximate Mach number and dynamic pressure were 0.048 and 656 Pa, respectively. Lift and pitching moment were evaluated by integrating surface pressures. The measurement of drag was again by wake survey, accomplished using a traversing rake of total pressure probes providing a reading every 2.54 mm. The rake was constrained to operate at a distance of approximately 21 in. downstream of the trailing edge. Pressures were measured using a PSI 8400 electronic pressure scanner with a range of 6.89 kPa calibrated using a 6.89 kPa range precision unit. More details concerning this historic facility may be found in Ref. 14.

## Results

Boundary corrections were applied to the force data of the full-scale test using the method described in Ref. 13. Wake blockage, solid blockage, streamline curvature, and buoyancy were taken into account. Raw data from three angle-of-attack sweeps (runs) were combined and a least-squares fit applied. The fitted raw data were then corrected and are shown in the plots of Figs. 8–10 at the corrected angles of attack. The limit to the angle-of-attack range was governed by the ability to obtain wake drag data. The wake size with respect to the rake limited the range (uncorrected angle of attack) to $-0.5 < \alpha < 3.5$ deg, which fell within the aforementioned limit of less than 15% correction to any value ($C_l$, $C_d$, $C_m$, and $\alpha$).

**Table 1 Summary of test results**

| $\alpha$, deg | $C_l$ | $C_d$ | $C_m$ | $X_{cp}/c$ |
|---|---|---|---|---|
| −4 | 0.043 | 0.076 | −0.077 | 2.041 |
| −2 | 0.325 | 0.026 | −0.134 | 0.662 |
| 0 | 0.591 | 0.015 | −0.145 | 0.495 |
| 2 | 0.830 | 0.011 | −0.142 | 0.421 |
| 4 | 1.030 | 0.013 | −0.143 | 0.389 |
| 6 | 1.180 | 0.037 | −0.128 | 0.358 |
| 8 | 1.269 | —— | −0.114 | 0.340 |
| 9.5 | 1.287 | —— | −0.126 | 0.348 |
| 10 | 1.280 | —— | −0.153 | 0.370 |
| 12 | 1.215 | —— | −0.200 | 0.415 |
| 14 | 1.049 | —— | −0.207 | 0.447 |

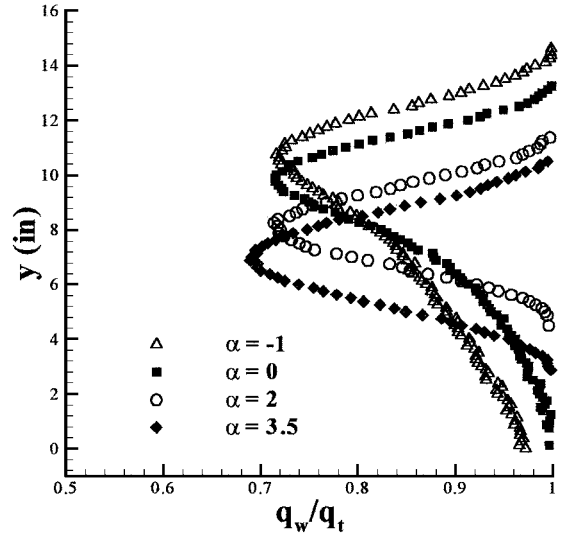


**Fig. 7 Sample wake data (full scale).**

Wake surveys from the full-scale test are shown in Fig. 7 plotted as wake position vs the ratio of dynamic pressure in the wake, $q_w$, to the freestream tunnel dynamic pressure $q_t$. The $\alpha = -1$ deg case illustrates a wake beyond the limits of the rake. The full-scale pitching moment data were found to be in error following the test, and the primary error source could be attributed to deflections in the mounting hardware.

The third-scale wake measurements were of similar shape for the corresponding angles of attack. The third-scale test results, the compilation of six runs, are presented raw and uncorrected. Corrections were omitted for two reasons: 1) Drag measurements were repeatable to a maximum of $\alpha = 6$ deg; however, drag values were required for the correction algorithm over the full pitch range. 2) The boundary corrections at the lower angles of attack were negligible.

### Forces and Moments

The polars of Figs. 8–10 summarize the lift, drag, and pitching moment data, which are tabulated with center of pressure calculations in Table 1. Correlation between the two models appears to be reasonable in all cases. Note that there are fewer points shown for the third-scale drag results vs the lift and pitching moment. A portion of the drag data was eliminated due to equipment problems with the rake wake instrumentation. From the third-scale data, the maximum lift coefficient was found to be approximately 1.3 at an angle of attack of 9.5 deg. A minimum drag coefficient of about 0.010 was measured using the full-scale model, whereas the third-scale model showed a slightly higher value. These values must then be weighed with the uncertainty level of the test as presented in a later section. The zero-lift angle of attack occurs at approximately $\alpha = -4.0$ deg; the minimum drag at $\alpha = 1.6$ deg. The lift curve slope measured using the full-scale model is measurably steeper than the third-scale model and is believed to represent the influence of the fabric deflection in comparison with the solid surface model.

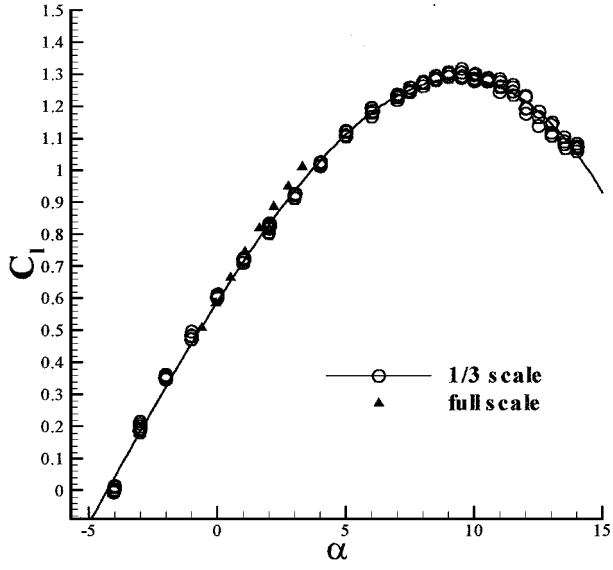


Fig. 8 Lift polar.

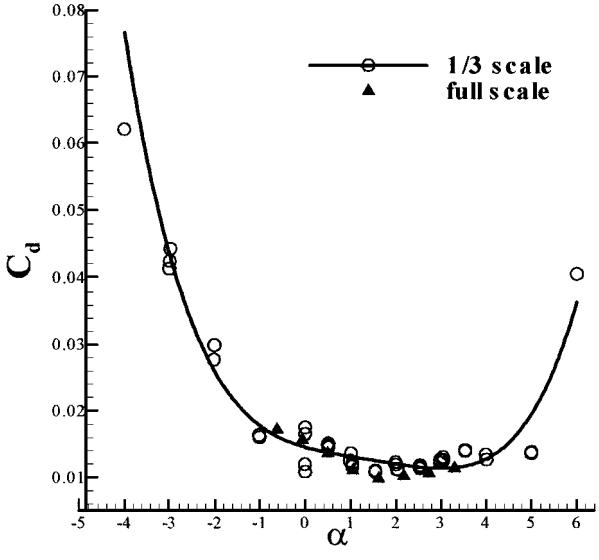


Fig. 9 Drag polar.

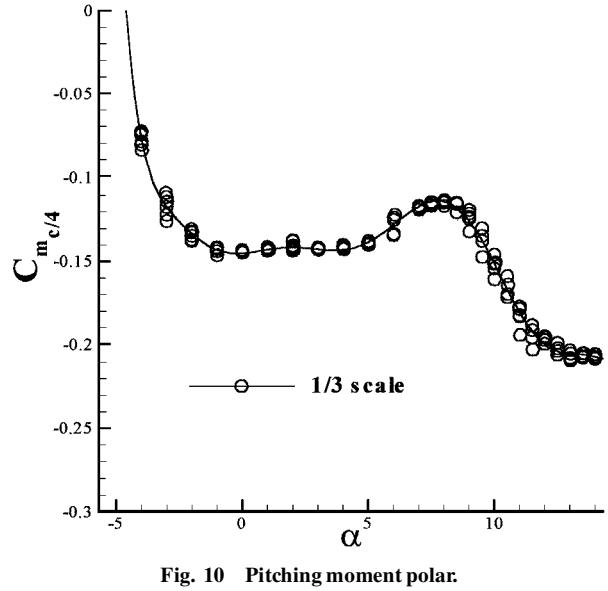


Fig. 10 Pitching moment polar.

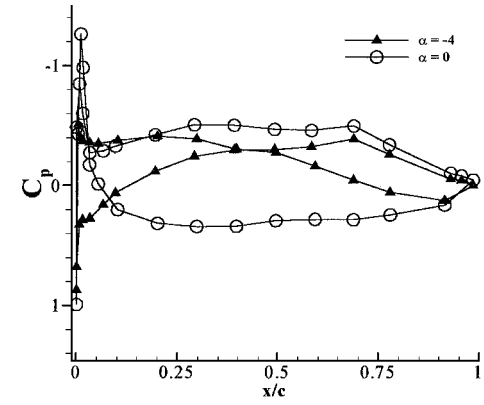


Fig. 11 Pressure distributions for $\alpha = -4$ and 0 deg.

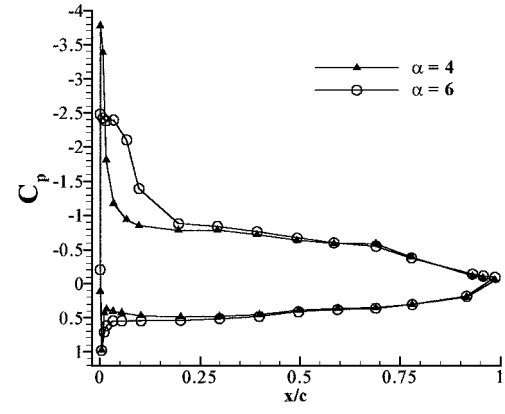


Fig. 12 Pressure distributions for $\alpha = 4$ and 6 deg.

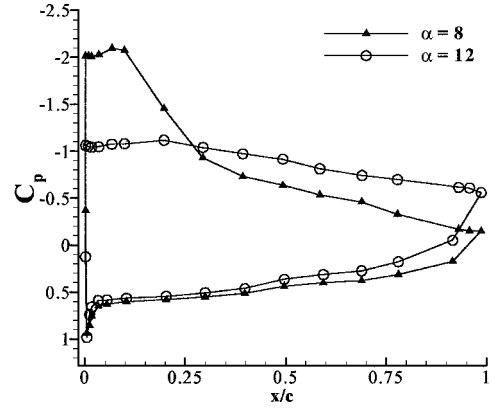


Fig. 13 Pressure distributions for $\alpha = 8$ and 12 deg.

### Pressure

Pressure data are presented in coefficient form for the 31 surface orifices. Note that the aftmost orifice was located in the relatively thick trailing edge. Figures 11–13 show representative pressure distributions from a single run as the model was pitched from zero lift through stall. No lift hysteresis was noted on returning the model to a zero-lift condition.

### Flow Visualization

Woolen tufts were glued to the top and bottom surfaces of the full-scale model and were filmed through the tunnel ceiling and sidewall windows. Optical access to the third-scale model was limited to the airfoil top surface where linen thread tufts were attached and filmed. Table 2 summarizes the results from the surface flow visualization studies. The term reversal refers to tufts flowing in a direction opposite to the freestream flow direction that occurs, for example, in a recirculation bubble. Fluttering indicates motion of

**Table 2 Flow visualization results**

| $\alpha$ | Result |
|---|---|
| | *Bottom surface* |
| −4 | Reversal at LE to $x/c = 0.3$–$0.4$ |
| −3 | Reversal at LE to $x/c = 0.3$–$0.4$ |
| −2 | Reversal at LE to $x/c = 0.2$–$0.25$ |
| −1 | Reversal at LE to $x/c = 0.05$–$0.1$ |
| 0 | Reversal at LE to $x/c = 0.05$ |
| 1–14 | All tufts attached |
| | *Top surface* |
| 1 | Reversal at LE, fluttering TE |
| 6.5 | All tufts fluttering gently |
| 8 | Pronounced fluttering entire upper surface |
| 10 | First tuft reversal at TE |
| 14 | Entire surface shows reversal |

**Table 3 Uncertainty in force and moment measurements**

| Coefficient | $\alpha$, deg | Bias | Precision | Mean | Uncertainty |
|---|---|---|---|---|---|
| | | *Full scale* | | | |
| Drag | 2 | 0.0004 | 0.0003 | 0.0100 | 0.0005 |
| Lift | 2 | 0.0066 | 0.0141 | 0.8660 | 0.0156 |
| | | *Third scale* | | | |
| Pitching moment | 0 | 0.0051 | 0.0016 | −0.1445 | 0.0053 |
| | 2 | 0.0051 | 0.0005 | −0.1424 | 0.0052 |
| | 7 | 0.0052 | 0.0007 | −0.1180 | 0.0052 |
| Lift | 0 | 0.0090 | 0.0141 | 0.6069 | 0.0167 |
| | 2 | 0.0092 | 0.0021 | 0.8220 | 0.0094 |
| | 7 | 0.0099 | 0.0066 | 1.2300 | 0.0119 |

the tufts and, when pronounced, indicates large-scale separation is present.

## Experimental Uncertainty

An estimate of the experimental uncertainty for the force and moment coefficients was calculated using the Ref. 15 standard for wind-tunnel data uncertainty and is summarized in Table 3. Precision was evaluated by repeated measurements and was calculated for a 95% confidence level. Bias was evaluated using existing facility instrument calibration data.

## Discussion

An estimate for the angle of attack (excluding power effects) required for level flight (cruise) at 64.4 kph at sea level is 3 deg, based on a vortex lattice program prediction. From the wind-tunnel test results presented here, the range of angle of attack over which the airfoil operates relatively efficiently is limited to 0–5 deg, bracketing the 3-deg cruise prediction. This assertion is based first on the flow visualization studies, which show measurable separation on either surface outside these limits, as well as noting the lift-to-drag ratio, which, for instance, is above 70 for an angle of attack greater than 2 deg and less than 4 deg. Beyond this, the pitching moment polar of Fig. 10 shows that the aerodynamic center will start to move from the near quarter-chord position, whereas the drag polar shows a marked rise in drag outside these pitch limits. To understand what flow phenomena define the limits of performance, it is necessary to correlate the force, pressure, and flow visualization study results.

As for the lower limit, the wake data of Fig. 7 reveals the lower surface separation witnessed in the flow visualization studies at low angles of attack. A recirculation bubble forms just aft of the leading edge and grows in size as the angle of attack is decreased from positive values. The influence of this bubble may be seen in the wake spreading of Fig. 7. The signature of this lower surface recirculation region may also be seen in the pressure distribution of Fig. 11. At $\alpha = 0$ deg, the bubble influence is seen as a low-pressure region near the leading edge. As the angle of attack approaches $\alpha = -4$ deg, this low-pressure region extends over most of the bottom surface and (as seen in Fig. 10) results in an increasingly nose-up moment relative to the cruise condition value.[16,17]

The upper limit in angle of attack is governed by top surface separation. The extremely adverse pressure gradient resulting from the rather blunt leading-edge geometry suggests a high probability of a laminar separation bubble followed by turbulent reattachment.[10,18] The tuft study supported this supposition in that reversed flow was shown just aft of the leading edge for small positive angles of attack. Unfortunately, optical access at LTPT did not allow viewing of the leading edge beyond approximately $\alpha = 4$ deg. The pressure distributions of Figs. 11–13 appear to show the growing size of the leading-edge (LE) separation bubble. For instance, consider the attenuated suction peak of $\alpha = 6$ deg vs 4 deg and then the subsequent development of a constant pressure region over the first 10–15% of the top surface shown in the 8-deg case. The tuft study showed large-scale separation with flow reversal at the trailing edge (TE) for $\alpha = 10$ deg. This is supported by the pressure distribution at $\alpha = 12$ deg showing the constant pressure region characteristic of a fully separated flow. As the angle of attack approaches stall, the pitching moment is increasingly nose-up until approximately $\alpha = 8$ deg, where it reaches a local maximum and then becomes increasingly nose-down.

The effect of fabric deformation on airfoil performance within the normal operating range does not appear to be dramatic.[19] Lift and drag values obtained from the two different models correlate well and when considering the experimental uncertainty may be indistinguishable. One interesting observation was made when comparing the measured lift curve slope of the two tests. Clearly, the full-scale data indicate a higher value (of $dC_l/d\alpha$) over the measured range. Observations during full-scale tests revealed a slight billowing of the upper surface fabric particularly over the positive angle-of-attack range. One possible explanation is that, as the loading increases over the top surface of the airfoil, the unsecured fabric assumes a slightly thicker and more highly cambered shape, gradually shifting the lift polar. By analogy, consider an airfoil with a plain flap and the hypothetical data of Fig. 14. The solid dark line represents the lift curve for the plain airfoil with zero flap deflection; the dashed lines represent the lift curves for increasing values of flap deflection (increased camber).[16,17,20] If the flap were deflected incrementally as the angle of attack was increased, the effect would be to shift the lift curve slope to the thin solid line. A similar process may occur on the Model B airfoil as the fabric deflects under load to a greater camber with each increment in angle of attack.

Comparisons with the original Wright wind tunnel measurements of 1901 were made using the measured lift and drag data of the current test. A numerical lifting line model was developed using a rectangular wing of aspect ratio 6. The angle of attack was increased until the first section reached the measured maximum section lift coefficient of 1.3, which produced a maximum lift coefficient for the wing of approximately 1.11 (Refs. 17 and 21). The lift slope was calculated using the Helmbold equation of Ref. 17. These two limits are shown with the original 1901 Wright lift data in Fig. 15. Lift-to-drag ratios were calculated using the recent data corrected for aspect ratio and revealed a value of approximately 14.8 at an angle of attack of 5 deg, compared to the Wright's reported value of 8.45 for the number 18 airfoil and 9.26 for the number 12. The Wright's original wind tunnel and balance provided representative lift predictions despite that tests were conducted at very low Reynolds numbers

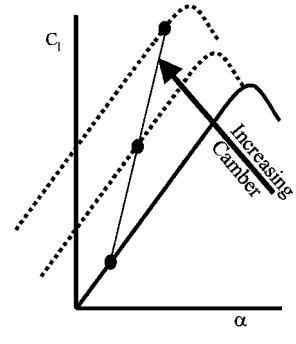


**Fig. 14 Effect of upper surface fabric deformation on lift polar.**

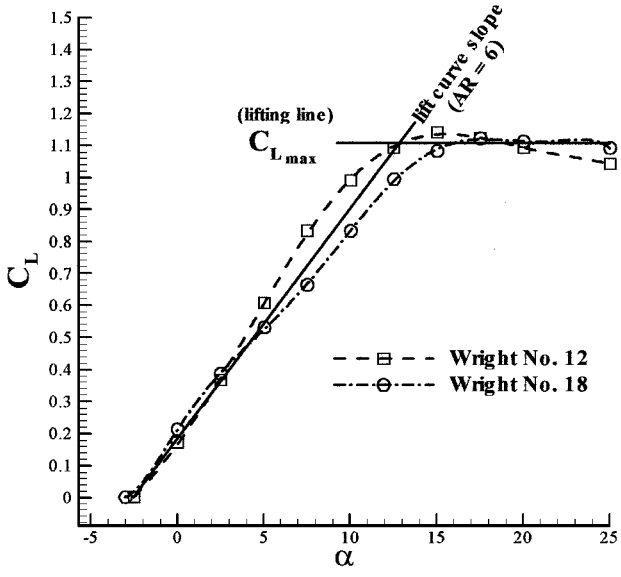


**Fig. 15 Comparisons to Wright 1901 wind-tunnel models.**

($5.8 \times 10^4$ vs $2.6 \times 10^6$ of the current test) with crude models by today's standards.

## Conclusions

Wind tunnel tests on the Wright Model B Flyer airfoil have been conducted to document aerodynamic behavior. The section was found to be relatively efficient over an angle-of-attack range from approximately 0 to 5 deg. A maximum lift coefficient of 1.30 was measured at an angle of attack of 9.5 deg. The minimum drag coefficient of 0.010 was found at an angle of attack of approximately 1.6 deg. Pitching moment about the quarter chord was relatively constant over the angle-of-attack range of 0–5 deg, but developed nonlinear behavior outside these limits. Comparisons to the Wright tests of 1901 show very good correlation with predicted lift and fair correlation with drag measurements.

## Acknowledgments

The authors would like to acknowledge the financial and technical support provided by NASA Langley Research Center with special thanks to B. Crawford, J. Cruz, J. Kegelman, P. Phillips, F. Quinto, B. Sewall, and L. Yip. An equal debt of gratitude for financial and technical support is directed to Wichita State University, especially to B. Johnson and S. Miller, and their students G. Heim, G. Thumann, and V. Tumwa. M. Selig is thanked for consultation.

## References

[1]McFarland, M. W., *The Papers of Wilbur and Orville Wright, Including the Chanute–Wright Letters*, Vols. 1 and 2, McGraw–Hill, New York, 1953, pp. 99–118.

[2]Jakab, P. L., *Visions of a Flying Machine*, Smithsonian Inst. Press, Washington, DC, 1990, pp. 63–114.

[3]Lilienthal, O., *Der Vogelflug als Grundlage der Fliegekunst*, R. Gaertners Verlagsbuchhandlung, Berlin, 1889; see Isenthal, I. W., *Birdflight as the Basis of Aviation*, Longmans, Green, London, 1911, (English translation).

[4]Anderson, J. D., Jr., *A History of Aerodynamics and Its Impact on Flying Machines*, Cambridge Univ. Press, Cambridge, England, U.K., 1997, pp. 205–239.

[5]"The Wright Stuff," Part 4c, *WW I Aero Magazine*, May 1993.

[6]"Users Guide for AIRFOIL II," Airware, Inc., Canton, CT, 1989.

[7]"Aerodynamic Characteristics of Aerofoils I," NACA TR 93, 1921.

[8]"Nomenclature for Aeronautics," NACA TR 240, 1927.

[9]Loukianoff, G. S., "Trag flächen-Untarsuch ungen des aerodynamischen Laboratoriums der Technischen Hochschule Moskau," *Zeitschrift fur Flugtech und Motorluftschiffahrt*, Vol. 3, No. 12, 1912, p. 153.

[10]Schlichting, H., *Boundary Layer Theory*, 7th ed., McGraw–Hill, New York, 1979, pp. 220, 221.

[11]"The Unusual Records of the Stay-Tight Aeroplane Fabric," Goodyear Tire and Rubber Co., Akron, OH, 1912.

[12]Johnson, B. L., *Facility Description of the Walter H. Beech Memorial* $7 \times 10$ *Foot Low-Speed Wind Tunnel*, National Inst. for Aviation Research, rev. A, Oct. 1997.

[13]Barlow, J. B., Rae, W. H., and Pope, A., *Low Speed Wind Tunnel Testing*, 3rd ed., Wiley, New York, 1999, pp. 349–364.

[14]Stainback, C. P., Mcghee, R. J., Beasley, W. D., and Morgan, Jr., H. L., "The Langley Research Center's Low-Turbulence Pressure Tunnel," AIAA Paper 86-0762, 1986.

[15]*Assessment of Wind Tunnel Data Uncertainty*, AIAA Standard, S-071-1999, AIAA, Reston, VA, 1999, pp. 31–42.

[16]Abbott, I. H., and Von Doenhoff, A. E., *Theory of Wing Sections*, Dover, New York, 1959, pp. 80–110, 132.

[17]McCormick, B. W., *Aerodynamics, Aeronautics, and Flight Mechanics*, Wiley, New York, 1995, pp. 62, 63, 9, 116, 171.

[18]Selig, M. S., Guglielmo, J. J., Broeren, A. P., and Giguère, P., "Experiments on Airfoils at Low Reynolds Numbers," AIAA Paper 96-0062, 1996.

[19]Ward, K. E., "Characteristics of an Airfoil as Affected by Fabric Sag," NACA TN 428, 1932.

[20]Smith, A. M. O., "High Lift Aerodynamics," AIAA Paper 74-939, 1974.

[21]Katz, J., and Plotkin, A., *Low-Speed Aerodynamics*, 2nd ed., Cambridge Univ. Press, Cambridge, England, U.K., 2001, pp. 193–207.